White Rose Research Online

eprints@whiterose.ac.uk
https://eprints.whiterose.ac.uk
Universities of Leeds, Sheffield and York

Deposited via The University of York.

White Rose Research Online URL for this paper:
https://eprints.whiterose.ac.uk/id/eprint/154577/

Version: Accepted Version

Book Section:
Landi, Federica and O'Higgins, Paul (2020) Applying Geometric Morphometrics to Digital Reconstruction and Anatomical Investigation. In: Rea, Paul, (ed.) Advances in Experimental Medicine and Biology. Springer, Cham, pp. 55-71.

https://doi.org/10.1007/978-3-030-24281-7

Reuse
Items deposited in White Rose Research Online are protected by copyright, with all rights reserved unless indicated otherwise. They may be downloaded and/or printed for private study, or other acts as permitted by national copyright laws. The publisher or other rights holders may allow further reproduction and re-use of the full text version. This is indicated by the licence information on the White Rose Research Online record for the item.

Takedown
If you consider content in White Rose Research Online to be in breach of UK law, please notify us by emailing eprints@whiterose.ac.uk including the URL of the record and the reason for the withdrawal request.

UNIVERSITY OF LEEDS
University of Sheffield
UNIVERSITY of York

Chapter

Applying geometric morphometrics to digital reconstruction and anatomical investigation

Federica Landi[1], Paul O'Higgins[1]

[1]PalaeoHub, Department of Archaeology and Centre for Anatomical and Human Sciences, Hull York Medical School, University of York (UK).
Hyfl4@hyms.ac.uk

Abstract
Virtual imaging, image manipulation and morphometric methods are increasingly used in medicine and the natural sciences. Virtual imaging hardware and image manipulation software allows us to readily visualise, explore, alter, repair and study digital objects. This suite of equipment and tools combined with statistical tools for the study of form variation and covariation using Procrustes based analyses of landmark coordinates, geometric morphometrics, makes possible a wide range of studies of human variation pertinent to biomedicine. These tools for imaging, quantifying and analysing form have already led to new insights into organismal growth, development and evolution and offer exciting prospects in future biomedical applications. This chapter presents a review of commonly used methods for digital acquisition, extraction and landmarking of anatomical structures and of the common geometric morphometric statistical methods applied to investigate them: generalised Procrustes analysis to derive shape variables, principal component analysis to examine patterns of variation, multivariate

regression to examine how form is influenced by meaningful factors and partial least squares analysis to examine associations among structures or between these and other interesting variables. An example study of human facial and maxillary sinus ontogeny illustrates these approaches.

Keywords: Virtual imaging, Geometric morphometrics, medical investigation, maxillary sinuses, Procrustes shape analysis

1 Introduction

1.1 Imaging 3D anatomy

Virtual study of the anatomy of living and extinct species, our natural heritage, and that of our cultural products, such as artefacts and buildings, is dependent on the methodologies available to image, reconstruct and investigate them (Bourne, 2010; Weber and Bookstein, 2011; Profico et al., 2018). The digital revolution has provided a series of innovative and non-invasive tools for the study of objects and biological structures. In the past 20 years, through advances in mathematics, computer science and physics, digital acquisition of data representing the 3D form of objects has become cheap and readily available. Disciplines such as palaeontology (Sutton et al., 2016), anthropology (Weber, 2014), forensics, medicine (Howerton and Mora, 2008), archaeology (Luhmann et al., 2006) and geography (Smith et al., 2016) apply these techniques to questions in evolutionary biology, functional morphology, biological

anthropology, medicine, ancient artefacts, geomorphology and to teaching. The advent of modern digital technologies has made it possible to easily visualize, manipulate, alter and explore objects in fine detail and extract information that would hardly be accessible without damaging specimens. Additionally, they allow us to process large datasets and perform complex analyses very rapidly (Bruner and Manzi, 2006).

As digital image acquisition has become readily available and increasingly applied in science, the technologies and methods that facilitate the study of these images have also expanded (Goel et al., 2016; Toennies, 2017; Sadler, 2018). Computerised tomography (CT-scanning) is an important and commonly used imaging modality applied to the study of internal and external form. In acquiring images the object is exposed to x-rays from different directions (e.g. by rotating the x-ray source or object) while multiple x-ray detectors capture the data required to reconstruct a contiguous series of slices. These can then be reconstructed as a volume or a 3D surface mesh (Brenner and Hall, 2007; Mettler Jr. et al., 2000). The resulting volume is rendered as voxels with shades (levels) of grey reflecting the degree of attenuation and so, the radiodensity of each tissue, measured in Hounsfield units (Razi et al., 2014; Hounsfield, 1973; Mah et al., 2010). CT scanning is widely applied in medicine and biomedical research. It produces detailed volumetrically accurate images of internal and external structures but presents a few issues with regard to image quality. One such issue is that CT scans may

contain artefacts, defined as any systematic discrepancy between the CT reconstruction and the true attenuation coefficients of the object (Barrett and Keat, 2004). Physics-based artefacts result from the physical processes of beam hardening involved in the acquisition of CT data. Patient-based artefacts can be caused by the presence of high-density material such as metal. The CT-scan device can cause ring artefacts, due to imperfections in the detector elements such as a calibration error in the detector array, while helical and multisection artefacts are caused by the helical interpolation and reconstruction process. Whatever their nature, artefact presence can damage the final resolution of the slices and therefore impact segmentation, anatomical investigation and clinical diagnosis (Goerres et al., 2002; Sijbers and Postnov, 2004; Barrett and Keat, 2004). However, with modern hospital CT scanners and software good quality reconstructions, useful in many scientific and clinical contexts can readily be made (Fig. 1).

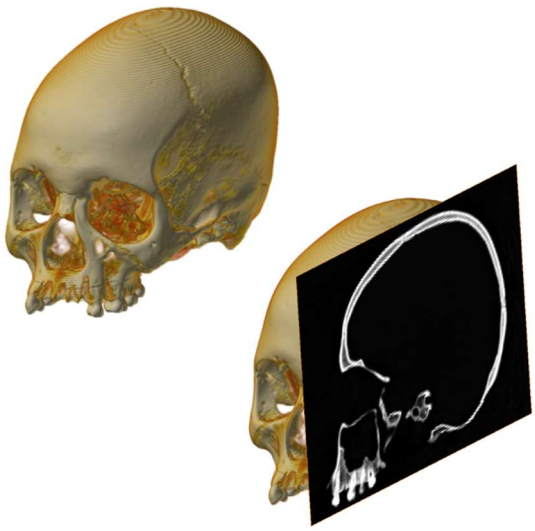

Fig. 1 Volume rendering of a human skull from a stack of CT-scans. An orthoslice is shown in the sagittal plane. Internal cavities and bone densities are clearly visible

Micro CT scanning is an increasingly common technique in biological work and is comparable to medical CT-scanning but uses a more focussed x-ray beam and detectors with small pixel patches to image on a smaller scale and at much higher resolution (Ritman, 2002). With current, commonly available microCT scanners objects as large as 200 millimetres in diameter can be scanned with pixel sizes as small as 100 nanometres. Feldkamp et al., (1989) noted that micro-CT offers advantages over histology in preserving sample integrity, being less time consuming and in readily allowing 3D structure to be appraised. However, exposure to high levels of ionizing radiation in micro-CT means that this approach is unsuitable for *in vivo* biological

work (Willekens et al., 2010). In the study of fossils and archeological material, micro-CT has largely replaced older and more invasive approaches used to remove sediment or isolate fragments (Cunningham et al., 2014).

Magnetic resonance imaging (MRI) is a cross-sectional imaging technique that uses the magnetic properties of materials to visualize structures in the body (Van Der Straeten, 2013). In brief, it differs from CT scanning in that no ionising radiation is used, rather, in medicine images are created using a strong magnetic field and radio frequency energy to visualise water content throughout the volume of the body region. In contrast to CT, MRI results in detailed images of soft tissues. Both CT and MRI techniques are volumetric methods, capturing internal morphology and allowing exploration of the internal anatomy of animals, organs and tissues.

Rather than the volume of an object, the form of the external surface is all that is required for many studies. One of the most commonly used approaches to surface digitisation is through the reconstruction of a 3D surface from a series of images in which the surface is illuminated by projection of either a single line of illumination (e.g. from a laser; Fig. 2) or a more complex pattern (stereoscopic structured light scanning) onto the surface. Both of these use one or multiple cameras to capture images of the projection, which appears distorted according to surface topography. A function is then used to reconstruct surface topography from these images and to represent it as a 3D polygon mesh. The camera and light source are placed

asymmetrically so that the device can assess depth as the bands of the light curve over the surface of the scanned item (Weber and Bookstein, 2011). Stereoscopic structured light scanning can be used to rapidly and non-invasively generate surface meshes of single objects (Niven et al., 2009). It is used in a wide range of research and museum applications to accurately record surface morphology (McPherron et al., 2009). However, it has limitations. If the object is reflective or lacking in surface texture, scanners will often fail to acquire and perform an accurate rendering of the surface (Gupta et al., 2011, Slizewski and Semal 2009). Further, stereoscopic structured light scanning is very sensitive to lighting conditions, camera placement and the number of images used to acquire the surface, which means that acquisition may need to be repeated several times until the right conditions for a particular object are found.

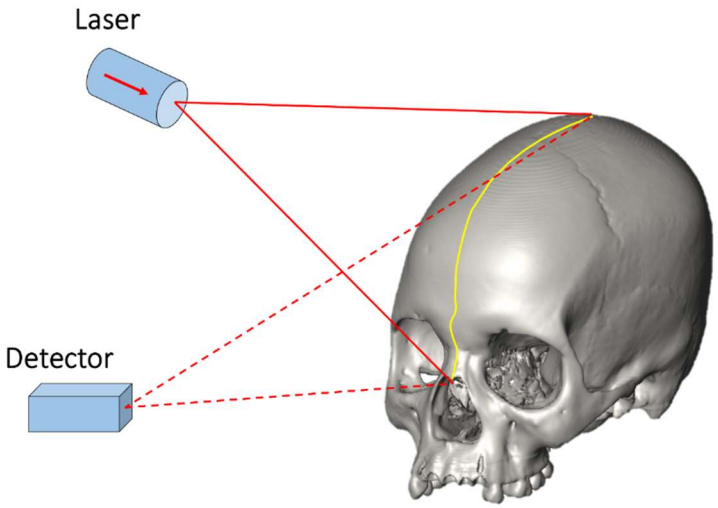

Fig.2 Schematic illustration of the principles of a laser scanner: a single line of laser light is projected on the surface of interest, reflected and received by the detector. This operation is repeated from multiple angles until the whole surface is scanned

Photogrammetry shares with light projection methods the capturing of a series of images from varying viewpoints as the basis for reconstructing three-dimensional 3D surface topology. It is not a new technique but has recently seen a substantial revival of interest in applications within the natural sciences (Bates et al., 2010; Falkingham, 2011; Evin et al., 2016; Buzi et al., 2018; Sadler 2018). Photogrammetry technology comes from computer science and uses stereo-reconstruction techniques to transform images (taken from multiple viewpoints, by moving the camera around the object or by rotating the object itself) in two to three dimensions (Fig. 3).

Photogrammetry identifies matching points between overlapping images taken from different viewpoints and uses the apparent movement of these points between images to reconstruct 3D surface topography (Verhoeven, 2011). It is not as accurate as projection methods (Katz and Friess, 2014), but Evin et al. (2016) show that it can produce results of acceptable accuracy and it has the benefit that by capturing surface texture maps photorealistic colour renderings can be generated.

Photogrammetry has wide applicability and offers portability and low equipment costs. It permits rapid data collection in the field due to its ease of use and allows the reproduction not only of isolated bones and archaeological artefacts but also of entire excavation sites as well as geo-referenced data for topographical, ecological and archaeological studies (Sapirstein, 2016). These factors and the fact that all that is needed is a good camera and software (e.g. Agisoft Photoscan, 2014, and increasing numbers of mobile phone apps) to capture and process the images and obtain coloured textured meshes add to its utility and applicability.

In photogrammetry, meticulous planning (and testing) of lighting conditions and of the scheme of photography are vital to ensure precise rather than simply aesthetically pleasing topographic reconstructions (Dellepiane et al., 2013). It is vital that lighting is even, to avoid blind spots and so, errors in the final 3D surface. In addition, a good camera with appropriate lens and settings are important to ensure accuracy (Nicolae et al., 2014).

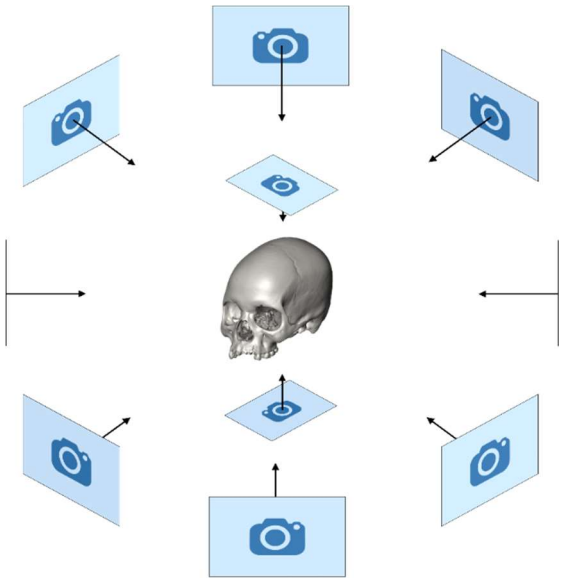

Fig 3 The construction of a photogrammetry model of a human skull. Pictures are taken around the object and from at least two different perspectives

1.2 Potential of 3D imaging in medical diagnosis and anatomical investigation

3D Medical imaging has evolved dramatically in the past few decades and is applied widely in detection and differential analysis of pathology and abnormalities (Doi, 2007; Sun, 2007; Chhabra et al., 2013; Schmidle et al., 2014). High-resolution, three-dimensional volumetric image data can be rapidly acquired and 3D visualization, multiplanar reformation and navigation through image volumes and surfaces underpins diagnosis in many fields of medicine. Digital

imaging applications have impacted care across a range of medical specialisations (e.g. Heiland et al., 2004; Joel et al., 2004; Bradley, 2008; Norouzi et al., 2014). Virtual methods of surgical simulation based on imaging data facilitate preoperative experimentation, improving planning of surgical treatment and potentially reducing patient risk (Meehan et al., 2003)

An emerging technique, rapid prototyping, can 3D print anatomical objects from 3D models. Physical printed models can be useful for surgeons in planning treatment as well as for training and teaching. Patients can also benefit from rapid prototyping by touching and looking at a physical model to improve their understanding of both the condition and the planned surgical intervention (Rengier et al., 2010). Thus, at present we are in the middle of a major transformation of how imaging is applied in medicine, through developments in virtual and physical reconstruction and modelling. These developments are opening up new possibilities for anatomical and medical investigation, detection and treatment (Tzou et al., 2011).

1.3 Quantification of morphology and analyses of variation: Geometric Morphometrics

Quantification of the form of virtual representations of anatomy, no matter how acquired, is necessary if we are to compare them in the context of diagnosis, planning and review. In this section we describe

how the use of linear and angular measurements to study form variation has been superseded in many applications in organismal biology by landmark based, geometric morphometric, methods. We illustrate how these landmark based approaches can be employed in biomedicine by applying them to the study of craniofacial growth in humans. We show how segmented images of human crania are reconstructed, landmarked and semilandmarked, and then how a model of maxillary growth can be derived from these data through a principal component analysis (PCA) and multivariate regression of form on centroid size. Further, we describe the application of 2-block partial least squares analysis (PLS) to assessment of the strength and nature of association between two related anatomical structures, and illustrate this by investigating how maxillary sinus form covaries with the form of the facial skeleton.

The sample comprises CT-scans of an ontogenetic series of modern humans (N=60). These were segmented semi-automatically using the software tool Avizo 9.0 (FEI Visualization). Because these scans are of dry bones, contrast is good between skull and air. Therefore, the initial segmentation was performed using a single global threshold, estimated by the histogram method (Pun, 1980) to maximize the inclusion of bone material in the resulting virtual reconstruction of the skulls. A second global threshold was applied to segment the maxillary sinus bone material. This semi-automatic segmentation often resulted in errors in the reconstruction of the orbital and nasal walls of the sinuses. This is because, when CT-scanning, the acquired

signal is sampled and not continuous and the effect of partial volume averaging becomes apparent after thresholding (Spoor et al., 1993).

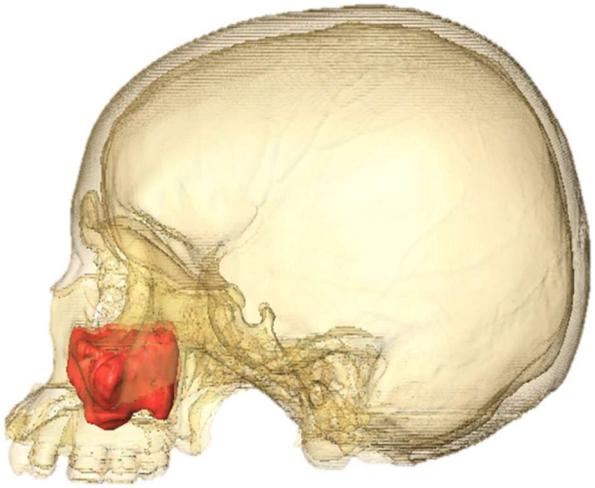

Fig 4 Mesh rendering of a maxillary sinus in a modern human adult specimen after segmentation and reconstruction

Therefore, thresholding of both cranium and sinuses was reviewed, slice by slice, so that the presence of unwanted elements (such as the scanning bed) and errors in segmentation (small holes in thin-bone structures such as the eye sockets and sinus medial walls) were manually fixed using the brush-tool available in Avizo 9.0. An example reconstructed cranium with highlighted maxillary sinus is shown in Fig 4.

Comparative morphological analysis has always played a central role in biological and medical studies (Adams et al., 2004). Qualitative descriptions of morphology have utility and a long-established history of application but are inherently subjective and lack repeatability. With the advent of multivariate statistical approaches in the mid-twentieth century, sets of linear measurements, indices and angles were used to explore shape variations and evaluate morphological differences between taxa (Sneath and Sokal, 1962; Blackith and Reyment, 1971; Bookstein, 1998).

Linear measurements between anatomical points (landmarks) individually describe the distance between them, while more than two measurements begin to describe the form, defined as the size and shape of an object. Multiple measurements taken on a sample can be submitted to multivariate analysis to assess and describe form variation. The use of linear measurements is well established and, with angular measurements formed the basis what became known as multivariate morphometrics (Blackith and Reyment,1971; Mardia et al., 1979). If we are interested in shape, measurements can be scaled before further analysis. Visualisation of the results of multivariate morphometric analyses of form or shape based on linear measurements is possible if the measurements are designed in such a way that the original geometry of the object can be reconstructed (e.g in Euclidean Distance Matrix Analysis, EDMA; Lele and Richtsmeier, 1991; Richtsmeier et al., 1993 a,b; Adams et al., 2004; and truss measures, Strauss and Bookstein, 1982).

However, the use of linear measurements or angles to describe shape is problematic. The key issue is that after scaling of interlandmark distances or using angles, the resulting shape spaces have undesirable statistical properties (independent isotropic error at landmarks does not result in isotropic distributions in the resulting shape spaces) and are a poor choice for statistical analysis (Rohlf, 2000).

The issue of how to compare objects based on landmark coordinates was the subject of intense debate and discovery in the 1980's and 1990's (Bookstein 1982; 1991; 1996; O'Higgins and Dryden, 1992; Richtsmeier and Lele, 1993; O'Higgins and Dryden, 1993; Marcus and Corti, 1996; Dryden and Mardia, 1998; Rohlf 1999) and led to the advent of geometric morphometrics (GM), a set of morphometric methods that caused a shift in the way in which biological structures were measured and investigated in many disciplines (Rohlf & Marcus, 1993; Slice et al., 2007). Thus, the statistical foundations of geometric morphometrics (GM) led to the development of a powerful set of tools for the investigation of shape variation and covariation that have been widely applied to the study of organismal growth, development and evolution (Roth & Mercer 2000; Cobb & O'Higgins, 2004; Mitteroecker et al., 2004; Goergen et al., 2017).

Increasing numbers of clinical and surgical studies have applied GM to study morphological changes in development, growth or pathology, to identify associations among skeletal units and between them and related soft tissues, to recognise proper and abnormal growth and

development and to document variation in anatomical structures (Hajeer et al., 2004; Singh et al., 2004).

In GM the geometry of an object, its form, is described using the landmark coordinates themselves, rather than measurements taken between them (Zelditch et al., 2012). To be comparable, these coordinates have to be equivalent in some sense, which means that they must correspond to points that are believed to have 'the same' developmental, evolutionary or functional significance (whichever is pertinent to the question) in different organisms (O'Higgins 1997; Bookstein, 1997 a; Oxnard and O'Higgins, 2009).

Landmarks can be placed on 2D (X-rays, pictures) and 3D surfaces (mesh rendering from CT-scan, laser scan or photogrammetry) and should be chosen to provide an adequate representation of the object under study in relation to the question at hand (O'Higgins 1997; Lele and Richtsmeier, 2001; Oxnard and O'Higgins, 2009). When equivalent points between specimens are scarce, semilandmarks (defined as those that lie on curves or surfaces but with ill defined exact location on the curve or surface; Bookstein, 1997 b; Mitteroecker & Gunz, 2009) can be applied, as long as a sufficient number of equivalent landmarks can be used as a fixed reference to control subsequent sliding over surfaces and curves to minimise error in the location of semilandmarks. The sliding procedure iteratively adjusts the positions of the semilandmarks until either the Procrustes distance or bending energy between the reference specimen (also estimated iteratively) and that being landmarked is minimal.

Minimisation of Procrustes distances takes the locations of all fixed landmarks equally into account (global form) to guide the sliding, whereas the minimisation of bending energy gives greater weight to landmarks near the surface or curve on which they are to be slid. The choice of Procrustes distance or bending energy leads to different eventual semilandmark positions and so, different estimates of differences among specimens. The choice should be guided by which criterion seems most appropriate to the question. Most often in applications to crania, minimisation of bending energy (see warping, below) has been preferred because this slides semilandmarks based on local rather than global aspects of form (Gunz et al., 2005). After sliding, landmarks and semilandmarks each have the same weight in subsequent statistical analyses (Gunz and Mitteroecker, 2013).

Figure 5 illustrates the landmarks and semilandmarks recorded on the 3D surface mesh of each cranium from the ontogenetic series described above. These cover the external and internal surfaces of the face, base and cranial vault. Six landmarks were also located on the surface of each maxillary sinus. Since the sinuses almost totally lack identifiable equivalent anatomical landmarks, five of these were defined with respect to the Frankfurt plane (most lateral, inferior, superior, anterior and posterior). The sixth is an anatomical landmark, at the ostium.

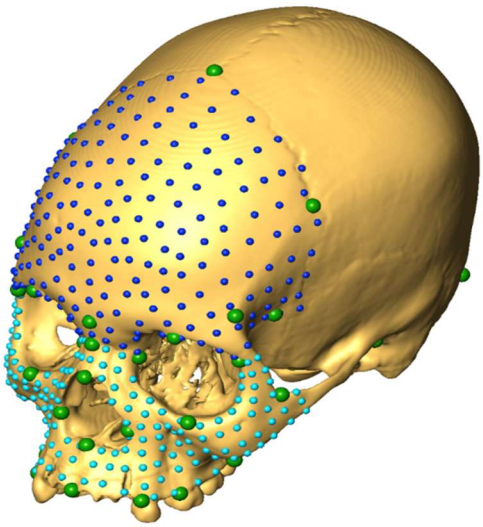

Fig 5 Landmark (green) and semilandmark configuration (light blue for the facial skeleton and dark blue for the frontal bone) used for the study of midfacial and sinus morphology shown on a human skull

Once landmarks have been collected the form of specimens can be compared pairwise, visually, in terms of warpings between them, or patterns of variation within the entire sample can be assessed using Procrustes based statistical analyses.

Warping of meshes representing surfaces or of volumes of specimens involves interpolation of differences in landmark configurations to the space in the vicinity of the landmarks, occupied by virtual objects representing surfaces or volumes. Thus, differences between two landmark configurations are used to smoothly warp surface meshes or volumes representing the anatomical structure on which the landmark configurations were taken. The two configurations are termed the reference configuration (the original object surface or volume) and the target configuration (into which the object will be warped). They could be two specimens or represent objects at opposite poles of a vector of interest arising from statistical analyses, as described below. In GM, warping is most commonly achieved using two (for 2D) or three (for 3D) thin plate splines (TPS) as interpolating functions. The thin plate spline comprises a uniform (uniform stretchings and shears) and a non-uniform component. It interpolates differences in relative landmark locations to the space between them, minimising a quantity from the non-uniform component known as the bending energy, analogised as the energy required to deform a thin, uniform metal sheet. The 'metal sheet' is constrained at landmark coordinates but otherwise free to adopt the form that requires the minimum bending energy. This leads to a smooth interpolation of the space between

landmarks (Mitteroecker and Gunz, 2009). As noted above bending energy is commonly minimized by the algorithm used to slide semilandmarks. This is because bending energy is larger for localised deformations than global ones of the same magnitude. Thus, so sliding of semilandmarks based on minimization of bending energy gives greater weight to minimization of localized 'errors' in their initial locations.

Transformation grids (Thompson, 1917) are often used to visualise local variations in shape differences between two landmark configurations as a deformation (Fig. 6). They are calculated using one thin plate spline per dimension (2, for 2D or 3 for 3D data). The grids can be interpreted as indicating how the space in the region of a reference shape might be deformed into that in the region of the target such that landmarks in the reference map exactly into those of the target. The graphical representation of shape differences resulting from these approaches is readily interpretable in 2D but less so in 3D, where warping of a surface or volume as a movie or a series of 'stills' may lead to better understanding of the nature and degree of form differences between configurations. Care should be taken, in balancing the visual appeal of transformation grids against the underlying assumptions (e.g. smooth interpolation) in their construction. From a biological perspective it is important to bear in mind that this mapping is purely mathematical, and it is based only on the locations of the original landmarks (O'Higgins, 2000).

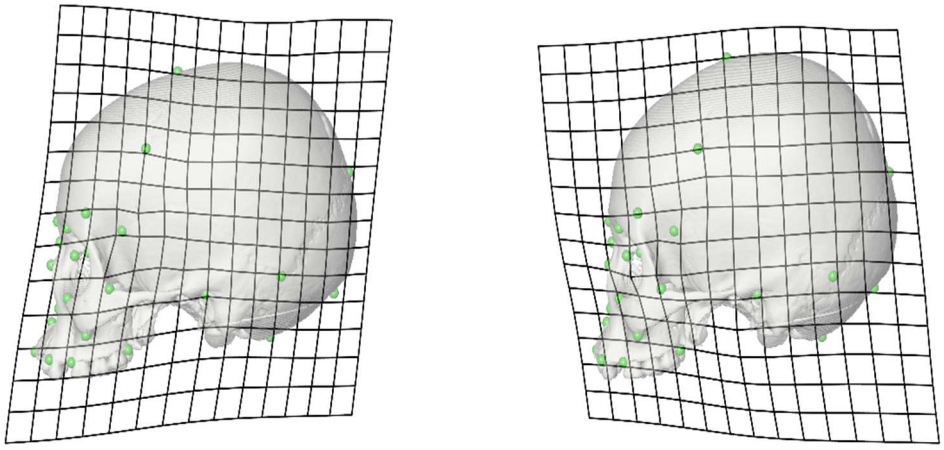

Fig 6 Transformation grids showing shape differences between two human crania. The grids are sited in the sagittal plane and the skulls are rendered semi-transparent so the grids can be viewed. A regular square grid was drawn over the mean (reference) of the two skulls and then it was deformed into each of them (targets). Thus, it shows equal and opposite deformations in each that indicate the local and global differences in shape between the two landmark configurations

Beyond visually comparing differences between pairs of landmark configurations, GM methods allow statistical analyses of variation and of covariation among different configurations of landmarks or between a configuration and other variables of interest. Landmark configurations differ among objects in form (size and shape) and in location and orientation. Geometric morphometric analyses aim to

investigate the shape of objects, regardless of 'size' (specifically, centroid size, see below), location and orientation in space. As such GM relies on the computation of shape differences among objects, expressed as Procrustes distances. These distances are estimated through generalized Procrustes analysis (GPA; Gower 1975; Kendall 1984; Rohlf and Slice, 1990; Goodall, 1991; Dryden and Mardia, 1993). This proceeds by standardising centroid size (the square root of the sum of squared distances of a set of landmarks from their centroid), position and orientation of the landmark configurations through registration. Squared distances between equivalent landmarks taken on all specimens are minimized by scaling, translating and rotating the individual's landmark configurations. Scaling is carried out such that the centroid size of each configuration is scaled to 1 by dividing the raw landmarks by the original configuration centroid size. Configurations are then superimposed at their centroids (the arithmetic mean of all landmark coordinates) and iteratively rotated with respect to each other to minimize the sum of squared distances of the specimens from the mean shape. In the first iteration, the specimens are aligned to an arbitrarily chosen one, normally the first, and once all configurations are best fitted to this, the sample mean of each coordinate is computed. In subsequent iterations the configurations are best fitted to the mean, which is recomputed and used in the next iteration. The algorithm stops when the sum of residuals from the mean reaches a minimum, usually after 3-5 iterations. The resulting registered landmark coordinates are

known as ‘shape coordinates’ and can be submitted to subsequent statistical analysis.

Kendall’s shape space (Kendall 1984; Goodall, 1991; Dryden and Mardia, 1993) is the shape space that would arise from full Procrustes fitting (scaling translation and rotation of a pair of configurations) of every specimen to every other one. For triangles it has the form of the manifold of a sphere of diameter 1, and for higher dimensions is a hypersphere. Kendall’s shape is discussed at length in statistical texts (Dryden and Mardia, 1993; Weber and Bookstein, 2011).

In practice, such a registration is not used often because it does not lend itself to visualisation of shape differences among a sample. Instead, GPA is carried out, as described above because this incorporates calculation of the mean shape, which can be warped to visualise results of statistical analyses. After GPA, specimens come to lie on the manifold of a hemisphere with radius =1, known as the hemisphere of GPA aligned coordinates (Rohlf and Slice, 1990). As long as variations are small, the scatter of points over this manifold will be concentrated and, for practical purposes, very similar to that on the manifold of Kendall’s shape space. The region of (Kendall’s or GPA) shape space that they occupy can be considered approximately linear and so, suitable for multivariate analyses using linear models (Dryden and Mardia, 1993). However, it is common to formally linearise the region of shape space occupied by the specimens under study by carrying out a tangent projection (Dryden and Mardia, 1993; Kent, 1994). This is rather like what cartographers

do, when drawing maps on flat sheets of paper, and like maps, they do not distort distances much over small areas near the point of tangency (the mean) but more so for distances at the periphery of a distribution.

The tangent projected shape variables are then submitted to statistical analyses pertinent to the question at hand. Centroid size differences are also of interest and these can be used to examine how shape covaries with centroid size in studies of allometry or combined with the shape data, as an extra column in the shape coordinate data matrix (Mitteroecker et a., 2004; Mitteroecker et al., 2013), allowing analyses of form (size and shape) differences or covariances with other factors using standard multivariate methods.

Ordination methods are often used to visualise the scatter of points representing specimens within the shape space. They allow groupings and modes of variation among specimens to be visualised. The most commonly applied ordination method in GM studies is principal component analysis (PCA). In this, new orthogonal (therefore independent and uncorrelated) variables, the principal components (PCs), are extracted from the matrix of shape variables previously computed using GPA (see above). These are linear combinations, (rotations of axes within the space) of the original variables, sorted by decreasing variance (Rohlf, 1986; Mitteroecker and Gunz, 2009; Zelditch et al., 2012; Klingenberg, 2013; Mitteroecker et al., 2013) and retain the relationships (distances) among points. They allow the scatter of points in the high dimensional space defined by the original

correlated variables to be appreciated in fewer dimensions defined by the first few uncorrelated PCs, while retaining as much as possible of the variance of the original dataset (Jolliffe, 2011). The modes of shape variation represented by the PCs can readily be visualised as warpings of points, transformation grids, surfaces or volumes as described above.

The plot in figure 7 shows the first two principal components from an analysis of right sided maxillary sinus form in modern humans (60 specimens ranging from 0 to 60 years). GPA and PCA were performed using the R package Morpho (Schlager, 2013). PC1 accounts for 80% of the total variance in form of the sample and this represents a large change in size and a change in shape with increasing age, while PC2 accounts for 6% of the total variance and does not order specimens by age. Warpings of landmarks and meshes representing the maxillary sinus surface drawn in position within example crania show that infant sinuses are narrow medio-laterally and elongated antero-posteriorly and that they mainly expand in the vertical dimension during ontogeny, paralleling the large increase in facial height that occurs during the same period.

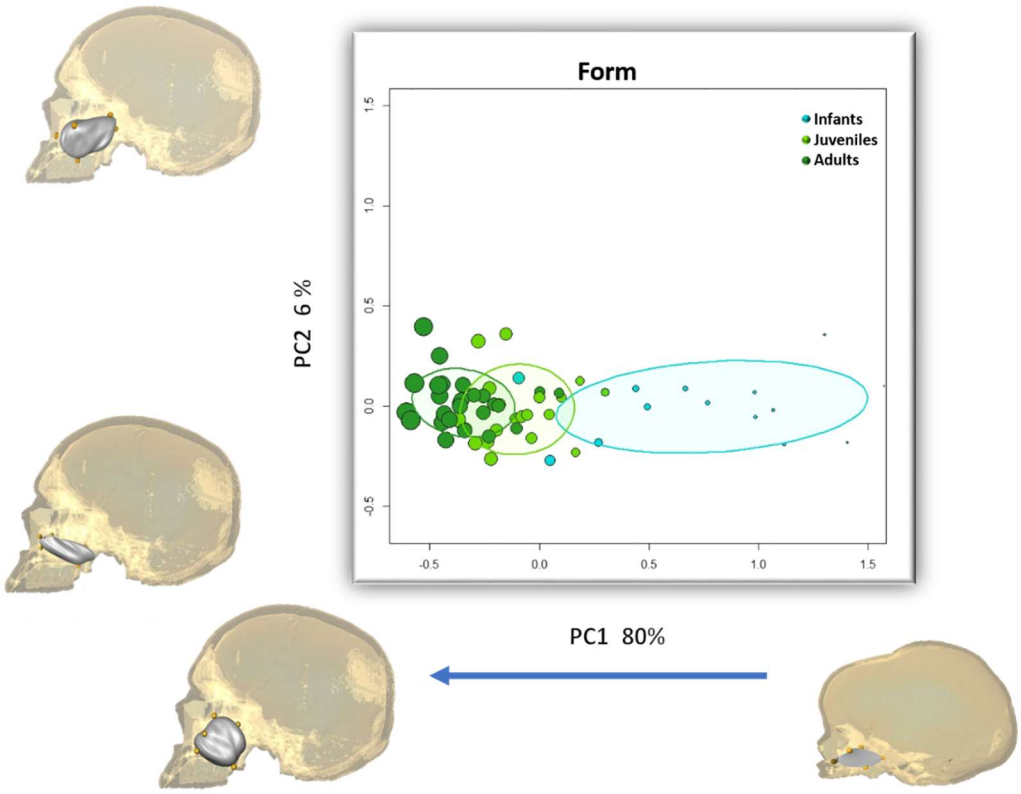

Fig 7 Principal component analysis. Plot of the first two principal components (86% of the total variance) of maxillary sinus form in a modern human sample. Age stages are indicated by colours: “light cyan” for infants up to the age of 6 years, “light green” for juveniles up to the age of 18 years and “dark green” for adults over the age of 18 years. The size of each point is proportional to the centroid size of each individual. The modes of sinus form variation represented by each principal component are shown (in grey) adjacent to each axis. These were drawn by warping the mean sinus to each extreme of each principal component, after which they were superimposed

Multivariate regression treats e.g. shape as being dependent on another variable of interest (such as size, time, diet etc), resulting in a vector of regression coefficients that indicates the change of shape per unit of change in the independent variable (Drake and Klingenberg, 2007; Klingenberg, 2013). Multivariate regression allows prediction of specimen shape for a given value of the independent variable and allows computation of the proportion of total shape variance explained by the independent variable. By predicting shapes at extremes of the regression vector and computing transformation grids, warped surfaces or object volumes as described above, the shape changes along a regression vector can be visualised.

A multivariate regression of sinus shape on centroid size, a study of ontogenetic allometry, was carried out using the sample of modern humans described above. The results show a significant ($p<0.001$) association between sinus shape and sinus size, but this is weak ($R^2= 0.18$), indicating that factors other than allometry are important in shaping sinus morphology during ontogeny. Visualisations of the shape differences between small and large sinuses are more or less identical to those shown in Fig 7 along PC1.

Where the association between one form and another or between a form and a set of interesting variables (e.g describing climate, ecology, behaviour) is of interest partial least squares analysis (PLS) is an appropriate method. Two-block partial least squares analysis (PLS) allows the covariation between two blocks of variables to be

quantified and visualised. It differs from regression analysis in that the two sets of variables are treated symmetrically rather than as one set of variables being dependent on the other (Rohlf and Corti, 2000). Two-block partial least squares analysis performed within a morphometric context is also called singular warp (SW) analysis (Bookstein et al., 2003). It computes the linear combination of two sets or "blocks" of shape variables (two landmark sets) that maximise explained covariance between blocks. It results in pairs of singular axes (also known as singular warps, singular vectors, singular axes or PLS axes) which maximise explained covariance and which, when plotted against each other, visualise the associations between blocks. The strength of the association between blocks can be quantified for each pair of axes by computing Pearson's correlation coefficient between the scores of each block (Hollander et al., 2013). To calculate the significance of this, a permutation test is used.

The proportion of total covariance explained by each pair of axes is also calculated. Beyond this, PLS allows the calculation of the proportion of total variance in each block explained by each singular axis for that block (Cardini, 2018). In reporting the results of PLS analyses, it is important to consider the strength and significance of correlations, the proportion of the total covariance explained by pairs of singular axes and the proportion of total variance in each block explained by each singular axis. This is because a strong association between blocks does not necessarily indicate that a large proportion of the variance of each block is explained by the analysis. Thus,

blocks can be strongly associated, but this association may account for a large or a small proportion of the total variance in each block. A strong and highly significant association that accounts for a very small proportion of the total variance, might have little real morphological or biological meaning. For visualization of the patterns of association in PLS analyses, the mean of each block (assuming both represent shape) is warped along each singular axis and the two warpings are presented, one for each block.

PLS was used to examine the association between maxillary sinus form and the form of the face during growth and development using the data described earlier. The 3D coordinates for each structure were first transformed to shape variables using GPA and, together with the ln of their centroid sizes, were submitted to a PLS. Figure 8 shows a plot of specimen scores on the first singular warps (SW1) of the sinus and the midface.

The correlation coefficient between the scores of each block on their respective SW1 is 0.94, $p<0.001$. 80% of the total variance in sinus form is associated with facial form and 81% of the total variance in facial form is associated with maxillary sinus form. Visualisations of the modes of associated form variation in each structure show similar changes to those observed in the PCA of figure 7: the sinus transforms from a relatively flat narrow structure to a vertically taller one while the face shows a degree of orbital enlargement, supero-inferior expansion of the zygomatico-maxillary region, an increase in nasal aperture and facial height.

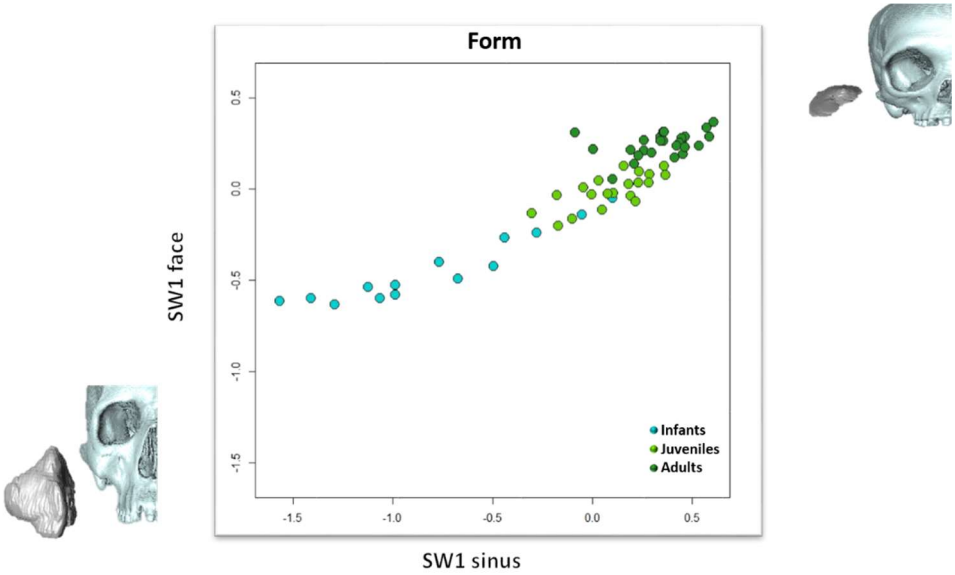

Fig 8 Partial least squares: a plot of the first pair of singular warps (SWs) from a PLS analysis of right sided maxillary sinus and facial form. Age stages are indicated by colours: "light cyan" for infants up to the age of 6 years, "light green" for juveniles up to the age of 18 years and "dark green" for adults over the age of 18 years. The inset figures to bottom left and upper right show warpings of the mean maxillary sinus and facial forms to the minimum and maximum limits of the scatter of points on each SW

1.4 Conclusions

The foregoing description of methods for imaging, reconstruction, visualisation and analysis of patterns of variation and covariation of

anatomical structures reflects the fact that we are entering an exciting period in the development of the anatomical sciences. By taking up the opportunities offered by the readily available state of the art hardware and software necessary to carry out this work, anatomical studies in relation to medicine can extend beyond the study of form to that of form variation and covariation and thus provide important data and tools for clinical assessment. By applying geometric morphometric methods, patterns of anatomical form variation and covariation can be quantified and used to assess pathology, patterns of normal and abnormal growth, development, and covariation of skeletal and soft tissue structures.

Thus, in this chapter, we illustrate the potential of modern imaging tools combined with GM by characterising normal ontogeny and ontogenetic interactions in the human craniofacial skeleton between the first few months of life and adulthood. This kind of study, carried out on extensive data, such as are held in the imaging departments of all major hospitals, could provide a modern equivalent of the growth standards developed by Tanner and co-workers in the middle of the last century (Tanner and Whitehouse, 1976). Furthermore, statistical models of variation can support the development of diagnostic and prognostic tools that facilitate identification of pathological form or form change. Thus Hajeer et al., (2004) used bilateral landmarks to study facial asymmetry caused by dentofacial deformities. They assessed the magnitude of 3D asymmetry of facial soft tissues before and after orthognathic surgery. 3D geometric morphometrics has also

been used to evaluate three-dimensional changes in nasal morphology in patients with unilateral cleft lip and palate, treated to correct naso-labio-alveolar deformities (Singh et al., 2005; Bugaighis et al., 2010). Further examples of applications include morphological analysis of neuroanatomical structures among adults (e.g. Free et al., 2001) or in a developmental context (e.g. Bookstein et al., 2001) to identify prenatal brain damage from alcohol and studies of thoracic volumes and breathing (Bastir et al., 2013; 2016).

In this chapter we focussed on long term changes in form due to growth and development but much shorter period changes in form, such as those due to motion, are also of interest clinically, and these too are amenable to GM analyses. Taking the heart as an example, its form alters with failure and its cyclic motion changes post myocardial infarction. A potentially useful application of GM is in the assessment of changes with failure or alterations in its cyclic motion as are being explored by Piras and co-workers (Piras et al., 2015).

Clearly the virtual domain presents many opportunities. We are just at the beginning of a phase of development of tools for imaging and analysis of images that promises practical technologies and applications with the potential to make a marked contribution in medical assessment, diagnosis, planning, and review.

References

Bourne, R. (2010). Fundamentals of digital imaging in medicine. *Medical Physics*, 37(7Part1), 3882-3882.

Weber, G. W., & Bookstein, F. L. (2011). *Virtual anthropology: a guide to a new interdisciplinar*y field. Springer, Vienna.

Profico, A., Bellucci, L., Buzi, C., Di Vincenzo, F., Micarelli, I., Strani, F., Manzi, G. (2018). Virtual anthropology and its application in cultural heritage studies. *Studies in Conservation*, 1-14.

Sutton, M., Rahman, I., & Garwood, R. (2016). Virtual paleontology—An overview. *The Paleontological Society Papers*, 22, 1-20.

Weber, G. W. (2014). Another link between archaeology and anthropology: virtual anthropology. *Digital Applications in Archaeology and Cultural Heritage*, 1(1), 3-11.

Howerton Jr, W. B., & Mora, M. A. (2008). Advancements in digital imaging: what is new and on the horizon? *The Journal of the American Dental Association*, 139, S20-S24.

Luhmann, T., Robson, S., Kyle, S. A., & Harley, I. A. (2006). *Close range photogrammetry: principles, techniques and applications*. Whittles, Scotland.

Smith, M. W., Carrivick, J. L., & Quincey, D. J. (2016). Structure from motion photogrammetry in physical geography. *Progress in Physical Geography*, 40(2), 247-275.

Bruner, E., & Manzi, G. (2006). Digital tools for the preservation of the human fossil heritage: Ceprano, Saccopastore, and other case studies. *Human Evolution*, 21(1), 33-44.

Goel, N., Yadav, A., & Singh, B. M. (2016). Medical image processing: A review. *Computational Intelligence on Power, Energy and Controls with their Impact on Humanity* (CIPECH) (pp. 57-62).

Toennies, K. D. (2017). *Guide to medical image analysis*. Springer, London.

Sadler J. (2018). *Capturing morphology*. Master thesis (unpublished), Hull York Medical School York (UK).

Brenner, D. J., & Hall, E. J. (2007). Computed tomography—an increasing source of radiation exposure. *New England Journal of Medicine*, 357(22), 2277-2284.

Mettler Jr, F. A., Wiest, P. W., Locken, J. A., & Kelsey, C. A. (2000). CT scanning: patterns of use and dose. *Journal of radiological protection*, 20(4), 353.

Razi, T., Niknami, M., & Ghazani, F. A. (2014). Relationship between Hounsfield unit in CT scan and gray scale in CBCT. Journal of dental research, dental clinics, dental prospects, 8(2), 107.

Hounsfield, G. N. (1973). Computerized transverse axial scanning (tomography): Part 1. Description of system. *The British journal of radiology*, 46(552), 1016-1022

Mah, P., Reeves, T. E., & McDavid, W. D. (2010). Deriving Hounsfield units using grey levels in cone beam computed tomography. *Dentomaxillofacial Radiology*, 39(6), 323-335.

Barrett, J. F., & Keat, N. (2004). Artifacts in CT: recognition and avoidance. *Radiographics*, 24(6), 1679-1691.

Goerres, G. W., Kamel, E., Heidelberg, T. N. H., Schwitter, M. R., Burger, C., & von Schulthess, G. K. (2002). PET-CT image co-registration in the thorax: influence of respiration. *European journal of nuclear medicine and molecular imaging*, 29(3), 351-360.

Sijbers, J., & Postnov, A. (2004). Reduction of ring artefacts in high resolution micro-CT reconstructions. *Physics in Medicine & Biology*, 49(14), N247.

Ritman, E. L. (2004). Micro-computed tomography—current status and developments. *Annual Review of Biomedical Engineering*, 6, 185-208.

Feldkamp, L. A., Goldstein, S. A., Parfitt, M. A., Jesion, G., & Kleerekoper, M. (1989). The direct examination of three-dimensional bone architecture in vitro by computed tomography. *Journal of bone and mineral research*, 4(1), 3-11.

Willekens, I., Buls, N., Lahoutte, T., Baeyens, L., Vanhove, C., Caveliers, V., ... & de Mey, J. (2010). Evaluation of the radiation dose in micro-CT with optimization of the scan protocol. *Contrast media & molecular imaging*, 5(4), 201-207.

Cunningham, J. A., Rahman, I. A., Lautenschlager, S., Rayfield, E. J., & Donoghue, P. C. (2014). A virtual world of paleontology. *Trends in ecology & evolution*, 29(6), 347-357.

Van Der Straeten, C. (2013). The use of magnetic resonance imaging (MRI) to evaluate hip resurfacing. *The Hip Resurfacing Handbook* (pp. 242-252). Elsevier, Amsterdam.

Niven, L., Steele, T. E., Finke, H., Gernat, T., & Hublin, J. J. (2009). Virtual skeletons: using a structured light scanner to create a 3D faunal comparative collection. *Journal of Archaeological Science*, 36(9), 2018-2023.

McPherron, S. P., Gernat, T., & Hublin, J. J. (2009). Structured light scanning for high-resolution documentation of in situ archaeological finds. *Journal of Archaeological Science*, 36(1), 19-24.

Gupta, M., Agrawal, A., Veeraraghavan, A., & Narasimhan, S. G. (2011). Structured light 3D scanning in the presence of global illumination. *Computer Vision and Pattern Recognition* (CVPR) (pp. 713-720).

Slizewski, A., & Semal, P. (2009). Experiences with low and high cost 3D surface scanner. *Quartär*, 56, 131-138.

Gernat, T., McPherron, S. P., Dibble, H. L., & Hublin, J. J. (2008). An application of structured light scanning to documenting excavated surfaces and in situ finds: examples from the Middle Paleolithic sites of Jonzac and Roc de Marsal, France. *Layers of Perception. Proceedings of the 35th International Conference on Computer Applications and Quantitative Methods in Archaeology (CAA).*

Bates, K. T., Falkingham, P. L., Rarity, F., Hodgetts, D., Purslow, A., & Manning, P. L. (2010). Application of high-resolution laser scanning and photogrammetric techniques to data acquisition, analysis and interpretation in palaeontology. *International Archives of the Photogrammetry, Remote Sensing, and Spatial Information Sciences*, 68-73.

Falkingham, P. L. (2011). Acquisition of high resolution three-dimensional models using free, open-source, photogrammetric software. *Palaeontologia electronica*, 15(1), 1-15.

Evin, A., Souter, T., Hulme-Beaman, A., Ameen, C., Allen, R., Viacava, P., Dobney, K. (2016). The use of close-range photogrammetry in zooarchaeology: Creating accurate 3D

models of wolf crania to study dog domestication. *Journal of Archaeological Science: Reports*, 9, 87-93.

Buzi, C., Micarelli, I., Profico, A., Conti, J., Grassetti, R., Cristiano, W., ... & Manzi, G. (2018). Measuring the shape: performance evaluation of a photogrammetry improvement applied to the Neanderthal skull Saccopastore 1. *ACTA IMEKO*, 7(3), 79-85.

Verhoeven, G. (2011). Taking computer vision aloft–archaeological three-dimensional reconstructions from aerial photographs with photoscan. *Archaeological prospection*, 18(1), 67-73.

Katz, D., & Friess, M. (2014). 3D from standard digital photography of human crania—a preliminary assessment. *American Journal of Physical Anthropology*, 154(1), 152-158.

Sapirstein, P. (2016). Accurate measurement with photogrammetry at large sites. *Journal of Archaeological Science*, 66, 137-145.

Agisoft, L. L. C. (2014). Agisoft photoscan. Professional Edition. St Petersburg, Russia.

Dellepiane, M., Dell'Unto, N., Callieri, M., Lindgren, S., & Scopigno, R. (2013). Archeological excavation monitoring using dense stereo matching techniques. Journal of Cultural Heritage, 14(3), 201-210.

Nicolae, C., Nocerino, E., Menna, F., & Remondino, F. (2014). Photogrammetry applied to problematic artefacts. *The International Archives of Photogrammetry, Remote Sensing and Spatial Information Sciences*, 40(5), 451.

Doi, K. (2007). Computer-aided diagnosis in medical imaging: historical review, current status and future potential. *Computerized medical imaging and graphics*, 31(4-5), 198-211.

Sun, Z. (2007). Multislice CT angiography in abdominal aortic aneurysm treated with endovascular stent grafts: evaluation of 2D and 3D visualisations. *Biomedical imaging and intervention journal*, 3(4).

Chhabra, A., Thawait, G. K., Soldatos, T., Thakkar, R. S., Del Grande, F., Chalian, M., & Carrino, J. A. (2013). High-resolution 3T MR neurography of the brachial plexus and its branches, with emphasis on 3D imaging. *American Journal of Neuroradiology*, 34(3), 486-497.

Schmidle, G., Rieger, M., Klauser, A. S., Thauerer, M., Hoermann, R., & Gabl, M. (2014). Intraosseous rotation of the scaphoid: assessment by using a 3D CT model—an anatomic study. *European radiology*, 24(6), 1357-1365.

Heiland, M., Schulze, D., Rother, U., & Schmelzle, R. (2004). Postoperative imaging of zygomaticomaxillary complex fractures using digital volume tomography. Journal of oral and maxillofacial surgery, 62(11), 1387-1391.

Joel, F., Leong, W. M., & Leong, A. S. Y. (2004). Digital imaging in pathology: theoretical and practical considerations, and applications. *Pathology*, 36(3), 234-241.

Bradley, W. G. (2008). History of medical imaging. *Proceedings of the American Philosophical Society*, 152(3), 349-361.

Norouzi, A., Rahim, M. S. M., Altameem, A., Saba, T., Rad, A. E., Rehman, A., & Uddin, M. (2014). Medical image segmentation methods, algorithms, and applications. *IETE Technical Review*, 31(3), 199-213

Meehan, M., Teschner, M., & Girod, S. (2003). Three-dimensional simulation and prediction of craniofacial surgery. *Orthodontics & craniofacial research*, 6, 102-107.

Rengier, F., Mehndiratta, A., Von Tengg-Kobligk, H., Zechmann, C. M., Unterhinninghofen, R., Kauczor, H. U., & Giesel, F. L. (2010). 3D printing based on imaging data: review of medical applications. *International journal of computer assisted radiology and surgery*, 5(4), 335-341.

Tzou, C. H. J., & Frey, M. (2011). Evolution of 3D surface imaging systems in facial plastic surgery. *Facial Plastic Surgery Clinics*, 19(4), 591-602.

Pun, T. (1980). A new method for grey-level picture thresholding using the entropy of the histogram. *Signal processing*, 2(3), 223-237.

Spoor, C. F., Zonneveld, F. W., & Macho, G. A. (1993). Linear measurements of cortical bone and dental enamel by computed tomography: applications and problems. *American Journal of Physical Anthropology*, 91(4), 469-484.

Adams, D. C., Rohlf, F. J., & Slice, D. E. (2004). Geometric morphometrics: ten years of progress following the 'revolution'. *Italian Journal of Zoology*, 71(1), 5-16.

Sneath, P. H., & Sokal, R. R. (1962). Numerical taxonomy. *Nature*, 193(4818), 855-860.

Blackith, R. E., & Reyment, R. A. (1971). *Multivariate morphometrics*.

Bookstein F. L., (1998). A hundred years of morphometrics. *Acta Zoologica Academiae Scientiarum Hungaricae*, 44: 7-59.

Mardia, K. V., Kent, J. T., & Bibby, J. M. (1979). *Multivariate Analysis*. Academic Press Inc., London.

Lele, S., & Richtsmeier, J. T. (1991). Euclidean distance matrix analysis: A coordinate-free approach for comparing biological shapes using landmark data. *American Journal of Physical Anthropology*, 86(3), 415-427.

Richtsmeier, J.T., Cheverud, J.M, Danahey, S.E., Corner, B.D., & Lele S., (1993 a). Sexual dimorphism of ontogeny in the crab-eating macaque (Macaca fascicularis). *Journal of Human Evolution*, 25(1), 1-30.

Richtsmeier, J. T., Corner, B. D., Grausz, H. M., Cheverud, J. M., & Danahey, S. E. (1993 b). The role of postnatal growth pattern in the production of facial morphology. *Systematic Biology*, 42(3), 307-330.

Strauss, R. E., & Bookstein, F. L. (1982). The truss: body form reconstructions in morphometrics. *Systematic Biology*, 31(2), 113-135.

Rohlf, F. J. (2000). On the use of shape spaces to compare morphometric methods. *Hystrix, the Italian Journal of Mammalogy*, 11(1).

Bookstein, F. L. (1982). Foundations of morphometrics. *Annual Review of Ecology and Systematics*, 13(1), 451-470.

Bookstein F. L., (1991). *Morphometric tools for landmark data: geometry and biology*. Cambridge University Press, Cambridge.

Bookstein, F. L. (1996). Combining the tools of geometric morphometrics. In *Advances in morphometrics* (pp. 131-151). Springer, Boston.

O'Higgins, P., & Dryden, I. L. (1992). Studies of craniofacial development and evolution. Archaeology in Oceania, 27(3), 105-112.

Richtsmeier, J. T., & Lele, S. (1993). A coordinate-free approach to the analysis of growth patterns: models and theoretical considerations. *Biological Reviews*, 68(3), 381-411.

O'Higgins, P., & Dryden, I. L. (1993). Sexual dimorphism in hominoids: further studies of craniofacial shape differences in Pan, Gorilla and Pongo. *Journal of Human Evolution*, 24(3), 183-205.

Marcus, L. F., & Corti, M. (1996). Overview of the new, or geometric morphometrics. In *Advances in morphometrics* (pp. 1-13). Springer, Boston, MA.

Dryden I. L., Mardia K. V. (1998). *Statistical shape analysis*. John Wiley & Sons, New York.

Rohlf, F. J. (1999). Shape statistics: Procrustes superimpositions and tangent spaces. Journal of Classification, 16(2), 197-223.

Rohlf, F. J., & Marcus, L. F. (1993). A revolution morphometrics. *Trends in ecology & evolution*, 8(4), 129-132.

Slice, D. E. (2007). Geometric morphometrics. *Annual Review of Anthropology*, 36.

Roth, V. L., & Mercer, J. M. (2000). Morphometrics in development and evolution. *American Zoologist*, 40(5), 801-810.

Cobb, S. N., & O'Higgins, P. (2004). Hominins do not share a common postnatal facial ontogenetic shape trajectory. *Journal of Experimental Zoology Part B: Molecular and Developmental Evolution*, 302(3), 302-321.

Mitteroecker, P., Gunz, P., Bernhard, M., Schaefer, K., & Bookstein, F. L. (2004). Comparison of cranial ontogenetic trajectories among great apes and humans. *Journal of Human Evolution*, 46(6), 679-698.

Goergen, M. J., Holton, N. E., & Grünheid, T. (2017). Morphological interaction between the nasal septum and nasofacial skeleton during human ontogeny. *Journal of anatomy*, 230(5), 689-700.

Hajeer, M. Y., Ayoub, A. F., & Millett, D. T. (2004). Three-dimensional assessment of facial soft-tissue asymmetry before and after orthognathic surgery. *British Journal of Oral and Maxillofacial Surgery*, 42(5), 396-404.

Singh, G. D., Levy-Bercowski, D., & Santiago, P. E. (2005). Three-dimensional nasal changes following nasoalveolar molding in patients with unilateral cleft lip and palate: geometric morphometrics. *The Cleft palate-craniofacial journal*, 42(4), 403-409.

Zelditch, M. L., Swiderski, D. L., & Sheets, H. D. (2012). *Geometric morphometrics for biologists: a primer*. Academic Press, New York and London.

O'Higgins, P. (1997). Methodological issues in the description of forms. *Fourier descriptors and their applications in biology*, 74-105.

Bookstein, F. L. (1997 a). Landmark methods for forms without landmarks: morphometrics of group differences in outline shape. *Medical image analysis*, 1(3), 225-243.

Oxnard CE, O'Higgins P (2009). Biology Clearly Needs Morphometrics. Does Morphometrics Need Biology? *Biological Theory*, 4(1), 1-14.

Lele, S. R., & Richtsmeier, J. T. (2001). *An invariant approach to statistical analysis of shapes*. Chapman and Hall/CRC, New York.

Bookstein, F. L. (1997 b). *Morphometric tools for landmark data: geometry and biology*. Cambridge University Press, Cambridge.

Mitteroecker, P., & Gunz, P. (2009). Advances in geometric morphometrics. *Evolutionary Biology*, 36(2), 235-247.

Gunz, P., Mitteroecker, P., & Bookstein, F. L. (2005). Semilandmarks in three dimensions. In *Modern morphometrics in physical anthropology* (pp. 73-98). Springer, Boston.

Gunz, P., & Mitteroecker, P. (2013). Semilandmarks: a method for quantifying curves and surfaces. *Hystrix, the Italian Journal of Mammalogy*, 24(1), 103-109.

Thompson, D. A. W. (1917). *On growth and form*. Cambridge Press, Cambridge.

Mitteroecker, P., Gunz, P., Windhager, S., & Schaefer, K. (2013). A brief review of shape, form, and allometry in geometric morphometrics, with applications to human facial morphology. Hystrix, the Italian Journal of Mammalogy, 24(1), 59-66.

O'Higgins, P., (2000). The study of morphological variation in the hominid fossil record: biology, landmarks and geometry. The Journal of Anatomy, 197(1), 103-120.

Gower, J. C. (1975). Generalized procrustes analysis. *Psychometrika*, 40(1), 33-51.

Kendall, D. G. (1984). Shape manifolds, procrustean metrics, and complex projective spaces. *Bulletin of the London Mathematical Society*, 16(2), 81-121.

Rohlf, F. J., & Slice, D. (1990). Extensions of the Procrustes method for the optimal superimposition of landmarks. *Systematic Biology*, 39(1), 40-59.

Goodall, C. (1991). Procrustes methods in the statistical analysis of shape. *Journal of the Royal Statistical Society*, *Series B (Methodological)*, 285-339.

Dryden, I. L., & Mardia, K. V. (1993). Multivariate shape analysis. Sankhyā: *The Indian Journal of Statistics, Series A*, 460-480.

Kent, J. T. (1994). The complex Bingham distribution and shape analysis. *Journal of the Royal Statistical Society, Series B (Methodological)*, 285-299.

Rohlf, F. J. (1986). Relationships among eigenshape analysis, Fourier analysis, and analysis of coordinates. *Mathematical Geology*, 18(8), 845-854.

Klingenberg, C. P. (2013). Visualizations in geometric morphometrics: how to read and how to make graphs showing shape changes. *Hystrix, the Italian Journal of Mammalogy*, 24(1), 15-24.

Jolliffe, I. (2011). Principal component analysis. In *International encyclopedia of statistical science* (pp. 1094-1096). Springer, Berlin.

Schlager, S. (2013). Morpho: Calculations and visualisations related to Geometric Morphometrics. *R package version 0.23*, 3.

Drake, A. G., & Klingenberg, C. P. (2007). The pace of morphological change: historical transformation of skull shape in St Bernard dogs. *Proceedings of the Royal Society B: Biological Sciences*, 275(1630), 71-76.

Rohlf, F. J., & Corti, M. (2000). Use of two-block partial least-squares to study covariation in shape. *Systematic Biology*, 49(4), 740-753.

Bookstein, F. L., Gunz, P., Mitteroecker, P., Prossinger, H., Schaefer, K., & Seidler, H. (2003). Cranial integration in Homo: singular warps analysis of the midsagittal plane in ontogeny and evolution. *Journal of Human Evolution*, 44(2), 167-187.

Hollander, M., Wolfe, D. A., & Chicken, E. (2013). *Nonparametric statistical methods*. Wiley & Sons, New York.

Cardini, A. (2018). Integration and modularity in Procrustes shape data: is there a risk of spurious results? *Evolutionary Biology*, 1-16.

Tanner, J. M., & Whitehouse, R. H. (1976). Clinical longitudinal standards for height, weight, height velocity, weight velocity, and stages of puberty. *Archives of disease in childhood*, 51(3), 170-179.

Bugaighis, I., O'higgins, P., Tiddeman, B., Mattick, C., Ben Ali, O., & Hobson, R. (2010). Three-dimensional geometric morphometrics applied to the study of children with cleft lip and/or palate from the North East of England. *The European Journal of Orthodontics*, 32(5), 514-521.

Bookstein, F. L., Sampson, P. D., Streissguth, A. P., & Connor, P. D. (2001). Geometric morphometrics of corpus callosum and subcortical structures in the fetal-alcohol-affected brain. *Teratology*, 64(1), 4-32.

Bastir, M., Martínez, D. G., Recheis, W., Barash, A., Coquerelle, M., Rios, L., ... & O'Higgins, P. (2013). Differential growth and development of the upper and lower human thorax. *PloS one*, 8(9), e75128.

Bastir, M., García-Martínez, D., Torres-Tamayo, N., Sanchis-Gimeno, J. A., O'Higgins, P., Utrilla, C., García Río, F. (2017). In vivo 3D A nalysis of Thoracic Kinematics: Changes in Size and Shape During Breathing and Their Implications for Respiratory Function in Recent Humans and Fossil Hominins. *The Anatomical Record*, 300(2), 255-264.

Piras, P., Teresi, L., Gabriele, S., Evangelista, A., Esposito, G., Varano, V., Puddu, P. E. (2015). Systo-diastolic lv shape analysis by geometric morphometrics and parallel transport highly discriminates myocardial infarction. In *International Workshop on Statistical Atlases and Computational Models of the Heart* (pp. 119-129). Springer, Cham.